Recyclable Conjugated Polyelectrolyte Hydrogels for Pseudocapacitor Fabrication

Jiang, Yan; Vázquez, Ricardo Javier; McCuskey, Samantha R.; Yip, Benjamin Rui Peng; Quek, Glenn; Ohayon, David; Kundukad, Binu; Wang, Xuehang; Bazan, Guillermo C.

DOI
10.1021/acsami.3c13137

Publication date
2024

Document Version
Final published version

Published in
ACS Applied Materials and Interfaces

ACS APPLIED MATERIALS & INTERFACES

www.acsami.org

Forum Article

Recyclable Conjugated Polyelectrolyte Hydrogels for Pseudocapacitor Fabrication

Yan Jiang, Ricardo Javier Vázquez, Samantha R. McCuskey, Benjamin Rui Peng Yip, Glenn Quek, David Ohayon, Binu Kundukad, Xuehang Wang, and Guillermo C. Bazan*

Cite This: https://doi.org/10.1021/acsami.3c13137

Read Online

ACCESS | Metrics & More | Article Recommendations | Supporting Information

ABSTRACT: In alignment with widespread interest in carbon neutralization and sustainable practices, we disclose that conjugated polyelectrolyte (CPE) hydrogels are a type of recyclable, electrochemically stable, and environmentally friendly pseudocapacitive material for energy storage applications. By leveraging ionic−electronic coupling in a relatively fluid medium, one finds that hydrogels prepared using a fresh batch of an anionic CPE, namely, Pris-CPE-K, exhibit a specific capacitance of 32.6 ± 6.6 F g^{-1} in 2 M NaCl and are capable of 80% (26.1 ± 6.5 F g^{-1}) capacitance retention after 100,000 galvanostatic charge−discharge (GCD) cycles at a current density (J) of 10 A g^{-1}. We note that equilibration under a constant potential prior to GCD analysis leads to the K^+ counterions in the CPE exchanging with Na^+ and, thus, the relevant active material Pris-CPE-Na. It is possible to remove the CPE material from the electrochemical cell via extraction with water and to carry out a simple purification through dialysis to produce a recycled material, namely Re-CPE-Na. The recycling workup has no significant detrimental impact on the electrochemical performance. Specifically, Re-CPE-Na hydrogels display an initial specific capacitance of 26.3 ± 1.2 F g^{-1} (at 10 A g^{-1}) and retain 77% of the capacitance after a subsequent 100,000 GCD cycles. Characterization by NMR, FTIR, and Raman spectroscopies, together with XPS and GPC measurements, revealed no change in the structure of the backbone or side chains. However, rheological measurements gave evidence of a slight loss in G' and G''. Overall, that CPE hydrogels display recyclability argues in favor of considering them as a novel materials platform for energy storage applications within an economically viable circular recycling strategy.

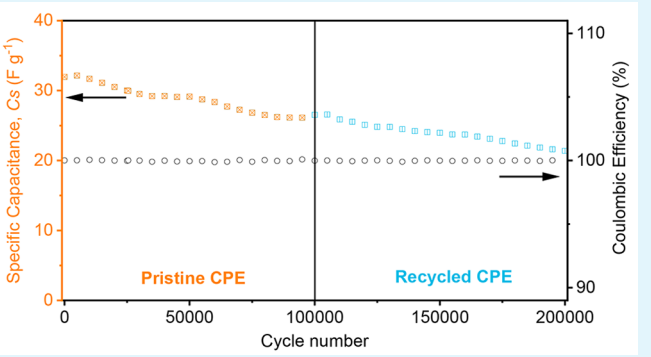

KEYWORDS: *conjugated polyelectrolytes, recyclable pseudocapacitive material, cycling stability, organic mixed ionic-electronic conductors, energy storage*

INTRODUCTION

Pseudocapacitors, also known as electrochemical capacitors, exhibit charge storage properties intermediate between those of electrical double-layer capacitors (EDLCs) and batteries.[1] Specifically, pseudocapacitors can be designed with higher energy densities than EDLCs, and higher power densities than batteries.[2] Pseudocapacitive materials store charge via mechanisms such as absorption, surface redox reactions, and intercalation in conjunction with reversible faradaic reactions adjacent to electrode surfaces.[3,4] Typical material classes include transition−metal oxides (composites), hydroxides, sulfides, carbides, and nitrides.[5−8]

Conjugated polymers are also under study as pseudocapacitive materials.[9−11] A diversity of chemical structures is available through which it is possible to modulate the voltage range of operation by controlling the effective conjugation length in the backbone as well as the electron affinity and ionization potential of individual structural units.[5,12−14] Doping mechanisms provide the basis for reversible redox activity and, when managed properly, can give rise to long-term cycling stability.[15,16] Moreover, solution-processability enables low-cost deposition to generate a variety of device architectures[17−20] and the incorporation of additives with the objective of enhancing pseudocapacitive figures of merit.[21,22]

Within the context of pseudocapacitive performance, conjugated polyelectrolytes (CPEs) have the potential to exhibit specific advantages relative to their neutral side chain analogs.[13] Pendant ionic functionalities are of particular relevance, since they can enhance ionic conductivity, stabilize doped states via electrostatic stabilization, enable water-

Special Issue: 25 Years of Conjugated Polyelectrolytes with a Focus on Applications

Received: September 3, 2023
Revised: December 1, 2023
Accepted: December 6, 2023

Scheme 1. Doping and De-doping of CPE-K together with a Schematic Illustrating the Recycling Study

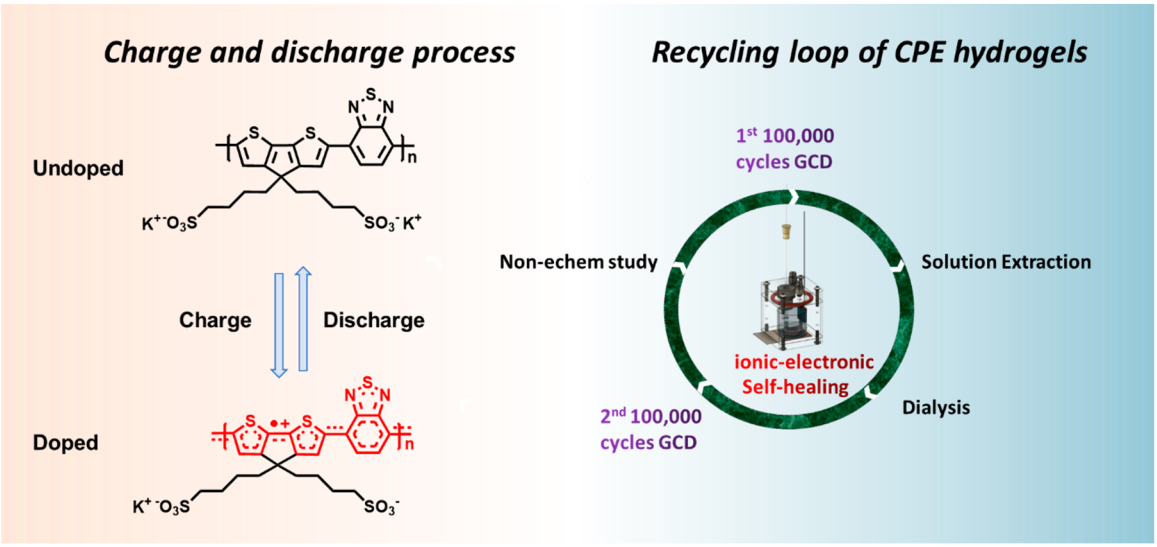

processability, and promote hydrogel formation.[23−25] One example is the case of CPE-K, see Scheme 1, which was initially studied in its hydrogel state to improve electron extraction from bioelectrogenic bacteria.[26,27] Subsequent studies demonstrated that a CPE-K biocomposite with *Shewanella oneidensis* MR-1 reversibly switched functions between electrical current generation in chronoamperometry mode and electrochemical energy storage as a pseudocapacitor.[28]

That CPE-K forms a pseudocapacitive hydrogel held together via non-covalent interactions led us to consider to what extent it is possible to recycle the material after operation.[29] Such considerations are relevant to materials selection, processing requirements, and recycling options in the context of sustainability.[23,30−32] Relevant properties in favor of recyclability include that hydrogels are self-healing, it is simple to extract the electrochemically active material through rinsing the charge collecting electrode with aqueous media, and dialysis provides a simple method of repurification; see Scheme 1.[33] In the recycling loop of CPE-K, we highlight the simplicity of dismantling, recycling, and repurification, with a "cradle to cradle" approach.[23] We show that electrochemical cells prepared with pristine CPE-K (Pris-CPE-K) in NaCl electrolyte retain 80% of their initial specific capacitance (C_s) after 100,000 GCD cycles at J = 10 A g^{-1}. The recycled material, obtained as the sodium salt (Re-CPE-Na) as a result of prior equilibration with NaCl (Re-CPE-Na), achieves a C_s (26.3 F g^{-1}) similar to the final conditions of the pristine CPE and demonstrates 77% capacitance retention after 100,000 GCD. No apparent chemical degradation of the backbone and side chains could be observed in the recycled polymer within the detection limits of various chemical structure characterization tools, which highlights the stability of the conjugated backbone and polar side chains under charge−discharge operations. Such recyclability highlights the promise of CPEs for designing reusable pseudocapacitive materials with potential utility in niche applications.

MATERIALS AND METHODS

Materials. Pris-CPE-K (Figure S1) was obtained via direct polymerization of the corresponding structural units via Suzuki cross-coupling conditions, while Pris-CPE-Na (Figure S2) and Pris-CPE-TBA (Figure S3) were obtained via dialysis of Pris-CPE-K in the presence of excess NaCl and tetrabutylammonium bromide (TBA-Br) following literature precedent.[34] Details on the NMR spectroscopy characterization are described in the Supporting Information. Re-CPE-Na was obtained after GCD measurements, as described in the recycling procedure. Re-CPE-TBA was prepared via the dialysis of Re-CPE-Na in the presence of TBA-Br. All materials were purchased from Sigma-Aldrich and used as received, unless otherwise indicated. The electrochemical cell was fabricated in the NUS Professional Workshop.

Cell Assembly. The cell for electrochemical testing comprised a three-electrode setup: a gold-coated working electrode well (area = 2 cm^2, depth = 247 ± 5 μm), a carbon felt counter electrode with dimensions of 2 cm × 2 cm (3.18 mm thick, 99.0%, Alfa Aesar), and a Ag/AgCl reference electrode filled with 3.5 M KCl (Latech Scientific Supply). Note that all measurements are reported relative to this reference electrode. The gold-coated electrodes were fabricated by Precision Semiconductor LLC in Santa Barbara, CA, by using heavily doped (ρ = 0.001−0.005 Ω cm) p + (boron) silicon wafers obtained from Addison Engineering Inc. Electrical contact was made with the working electrode by rubbing the posterior with gallium−indium eutectic and affixing to titanium foil (thickness 0.127 mm, 99.7% trace metals basis) using carbon tape. Titanium wire (0.25 mm) was connected to the carbon felt and twisted for 2−3 rounds to prepare the counter electrode, while the reference electrode was positioned adjacent to the working electrode. All electrochemical experiments were conducted using 2 M NaCl electrolyte under ambient conditions. Our choice of using NaCl over the KCl electrolyte is based on the higher initial C_s values in 2 M NaCl (Figure S4). To assemble the cell, the CPEs were diluted with Milli-Q water to a final concentration of 20 mg/mL. Subsequently, 100 μL of the CPE was deposited on the working electrode and frozen in a −80 °C freezer. After 2 min, the cell was assembled by putting a regenerated cellulose (RC) dialysis membrane (3.5 kDa molecular weight cutoff, Repligen) at the bottom of the chamber and twisting the screws on the bottom lid, followed by the addition of 15 mL of 2 M NaCl electrolyte in the chamber. (Figure S5 and S6)

Recycling Procedure. The CPE hydrogel from the electrochemical reactor was extracted from the electrode using Milli-Q water (pH = 6.00) until completely dissolved (as shown in Figure S7) and placed in snakeskin dialysis membrane tubing (3.5 kDa MWCO, Thermo Fisher Scientific).[34] The dialysis tubing was immersed in a beaker of Milli-Q water, and the water was changed every 12 h over the course of 4 days. The solution was transferred to a centrifuge tube, frozen at −80 °C for 1 h, and then promptly transported to a freezer dryer. After 4 days, a fluffy dark blue Re-CPE-Na solid was obtained.

https://doi.org/10.1021/acsami.3c13137
ACS Appl. Mater. Interfaces XXXX, XXX, XXX−XXX

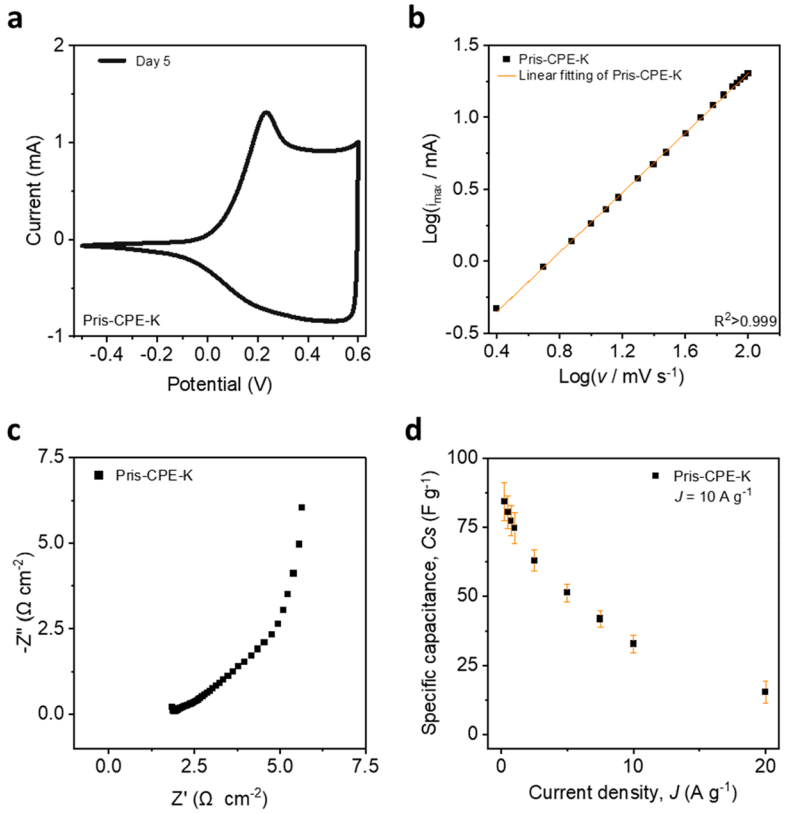

Figure 1. Electrochemical characterizations of cells prepared with Pris-CPE-K. (a) Cyclic voltammograms in 2 M NaCl measured at different times, potentials are referenced vs Ag/AgCl (3.5 M KCl), scant rate is 5 mV/s. (b) Linear fitting of $\log(i_{max})$ and $\log(v)$ on the 5th day. (c) Nyquist plot of EIS. (d) Specific capacitance at different current densities.

Electrochemical Characterizations. All electrochemical measurements were conducted using an electrochemical working station (BioLogic Potentiostat, VMP300) with EC-Lab software. Cyclic voltammetry (CV) tests were performed by scanning the potential from $E_{initial} = -0.5$ V to $E_{vertex} = +0.6$ V and back to $E_{final} = -0.5$ V at a scan rate of 5 mV/s. Sweep rate tests were undertaken by varying the scan rates from 2.5 to 100 mV/s. Potentiostatic electrochemical impedance spectroscopy (PEIS or EIS) tests were performed at a fixed potential of +0.3 V, covering a frequency range from 100 kHz to 100 mHz. EIS fitting process was carried out in EC-Lab. Chronoamperometry (CA) involved applying +0.3 V for 24 h prior to CV and EIS measurements, and the whole series of tests lasted for 5 days. The subsequent galvanostatic charge−discharge (GCD) studies were employed with a constant current (I) ranging from 0.5 mA (0.25 A g^{-1}) to 40 mA (20 A g^{-1}). The potential window of the capacitance measurements and cycling stability test was +0.2−0.6 V. Note that all error bars presented here are standard deviations.

Methods for Material Characterizations. Rheological and SEM measurements were performed by following previously reported protocols.[29] X-ray photoelectron spectroscopy (XPS) measurements were performed using the XPS Kratos AXIS Supra instrument, employing monochromatic Al Kα (1486.6 eV) X-ray beam excitation. The instrument was operated at 10 mA with a pass energy of 20 and 160 eV for usual narrow-scan and survey scan tests, respectively. The binding energy was calibrated based on the C 1s peak at 284.6 eV.[35] The background type in the region fittings was Tougaard, and the line shape for component fittings was LA (1.53, 243). Constraints in the full width at half-maximum (fwhm) were used to improve the accuracy of the relative intensities of the contribution of each peak in the model, which was conducted using the XPS fitting software CasaXPS. The uncertainty of fitting was evaluated by residual standard deviation (RSD) values. Fourier-transform infrared spectroscopy (FTIR) analysis was done using a Shimadzu spectrophotometer equipped with an attenuated total reflectance (ATR) attachment, the resolution of which was set at 16 cm^{-1}. Gel permeation chromatography (GPC) was conducted using a Waters Alliance e2695 HPLC system with a Waters 2414 Refractive Index detector. Two Agilent Polargel (M) columns (7.8 mm × 300 mm) and a Polargel Guard column were used. The mobile phase consisted of HPLC-grade DMF with 0.01% LiBr, and the flow rate was set at 1.0 mL/min. The detector and column temperatures were maintained at 50 and 60 °C, respectively. Calibration standards employed were Agilent PMMA Tripack, and quantification was performed using a solution of tetrabutylammonium congener with a concentration of 3 mg/mL.

RESULTS AND DISCUSSION

Electrochemical Performance of Cells Prepared with Pris-CPE-K Hydrogels. The electrochemical properties of cell-prepared pristine CPE-K (Pris-CPE-K) hydrogels were first examined via CV using 2 M NaCl electrolyte. These characteristics serve to subsequently determine the effect of recycling on the pseudocapacitive properties. Prior to CV or GCD measurements, the cells were equilibrated at 0.3 V until no further changes in the CV traces were observed. As shown in Figure 1a, the CV trace of cells prepared with Pris-CPE-K show square trace characteristics typical of a pseudocapacitor, consistent with the formation of a three-dimensional conducting network.[27] Variable scan rate CV was then used to untangle whether the charge storage process is more diffusion or surface controlled, as described in eq S1.[36] By taking the logarithm of each side of eq S1, we obtain eq 1,

$$\log(i_{max}) = \log(a) + b\log(v) \quad (1)$$

https://doi.org/10.1021/acsami.3c13137
ACS Appl. Mater. Interfaces XXXX, XXX, XXX−XXX

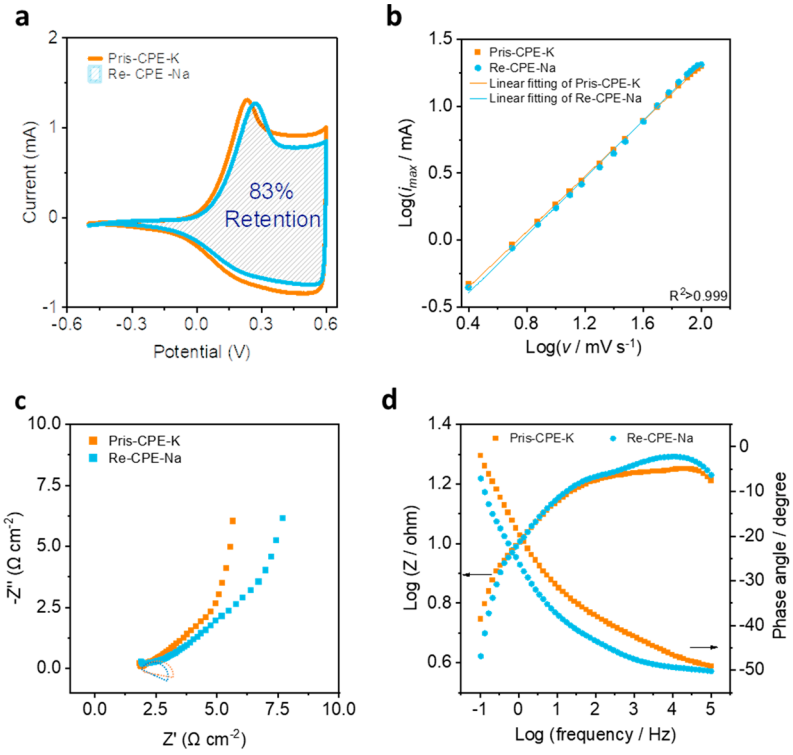

Figure 2. Electrochemical characterizations of cells prepared with Pris-CPE-K and Re-CPE-Na. (a) CV traces at 5 mV/s on the 5th day, (b) linear fitting of log(i_{max}) and log(v), (c) Nyquist plots of EIS, and (d) Bode plots of EIS.

Here, i_{max} is the maximum current (mA), v is the scan rate (mV/s), and a and b are constants. The b value in eq 1 corresponds to the slope of the current linear fitting, and its value is characteristic of diffusion- (b = 0.5) or surface-dominated (b = 1) processes. For cells prepared using Pris-CPE-K, we found that the kinetics of the charge storage process follow a surface-limited mechanism,[37] with a corresponding b value of 0.98 (Figure 1b and Figure S8).

Further insights into the charging process from the cells fabricated with Pris-CPE-K were sought by using electrochemical impedance spectroscopy (EIS). These measurements were carried out prior to GCD measurements.[38] We applied an equivalent circuit model, as shown in eq 2, to fit the impedance spectra:

$$R = R_s + R_{ct}/Q + Ma \tag{2}$$

where all the resistances in the Nyquist plots are normalized by the area of the working electrode cell. The solution resistance R_s in the Nyquist plot (Figure 1c) represents the equivalent series resistance (Ω cm^{-2}), which is the first intersection point with the real axis in the high-frequency section of the Nyquist plots. The second intersection with the real axis in the midfrequency section corresponds to the charge transfer resistance R_{ct} (Ω cm^{-2}), and the element Q demonstrates a constant phase element accounting for possible distortion from the electric double layer.[39] Additionally, the straight line terminated with an interfacial capacitor, with the phase angle at 45° gradually shifting to almost 90°, indicates the presence of a finite space Warburg (FSW) impedance,[40−42] which is represented by the modified restricted diffusion element Ma in eq 3,

$$Ma = R_d \frac{\coth(\sqrt[0.5a]{\tau j\omega})}{\sqrt[0.5a]{\tau j\omega}} \tag{3}$$

Here R_d is the restricted diffusion resistance (Ω cm^{-2}), τ is relaxation time (s) and ω is angular frequency (rad s^{-1}). We used the fitted EIS data to monitor differences in these elements (Figure S9 and Table S1) and determined the accuracy of the fittings based on the χ^2 values. From this modeling, we obtain an R_{ct} value for cells prepared with Pris-CPE-K of 1.0 ± 0.6 Ω cm^{-2}, indicating efficient electron transfer at the electrode−electrolyte interface. Furthermore, the FSW element provides a restricted diffusion resistance value of 9.0 ± 1.9 Ω cm^{-2}, which is a relatively low value and is reasonably attributed to facile ionic diffusion of electrolytes through the CPE hydrogel network.[43]

The charge storage capability of cells prepared with Pris-CPE-K was evaluated by measuring C_s at current loads from 0.25 to 20 A g^{-1}, as determined by GCD measurements. The calculation of C_s from GCD in a three-electrode configuration is obtained from eq 4:

$$C_s = \frac{I\Delta t}{m\Delta V} \tag{4}$$

C_s is the specific capacitance in F g^{-1}, I is the constant current (A), m is the mass of material (g), Δt is charging and discharging time (s), and ΔV is the operating potential window (V). At a low current density (J = 0.25 A g^{-1}), C_S = 84 ± 7 F g^{-1} (Figure 3a) and the IR drop is negligible, see Figure S10. A decrease in specific capacitance occurs at higher currents; for example, at J = 10 A g^{-1} one observes that C_s = 33 ± 3 F g^{-1} with an IR drop of 4.6 Ω. It is also worth mentioning that cycling stability is a significant requirement for practical implementation of pseudocapacitors.[15] Accordingly, we

https://doi.org/10.1021/acsami.3c13137
ACS Appl. Mater. Interfaces XXXX, XXX, XXX−XXX

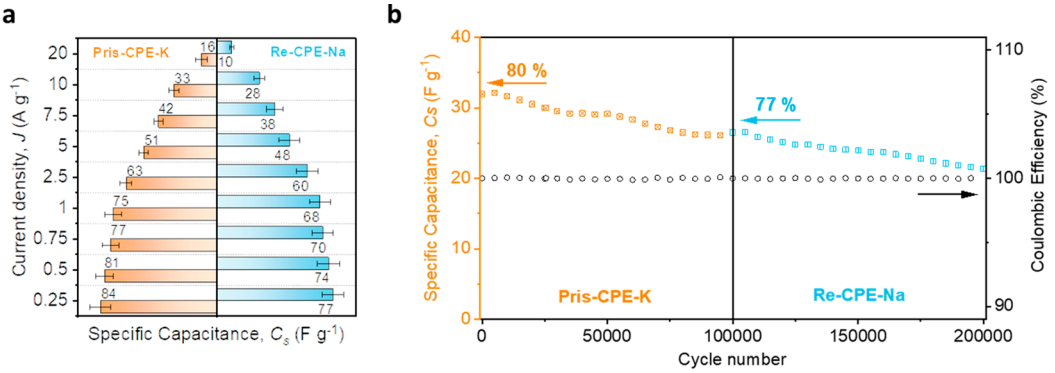

Figure 3. (a) Specific capacitance at different current densities, (b) specific capacitance (representative), and Coulombic efficiency (average of three groups) versus cycle numbers of cells prepared using Pris-CPE-K and Re-CPE-Na in 2 M NaCl.

determined that the cell fabricated with Pris-CPE-K demonstrated an final C_s of 26 ± 6.5 F g^{-1} corresponding to ~80% capacitance retention after 100,000 cycles GCD at 10 A g^{-1}, as shown in Figure 3b. We also carried out a set of experiments (as shown in Figure S11 and Figure S12) that measured up to 300,000 cycles at 10 A g^{-1} and determined that 50% of the original capacitance was retained, which is highly competitive compared to other conjugated polymer pseudocapacitors.[15]

It is worth noting that, as shown in Figure S13, rheological measurements of the hydrogels show that the storage moduli (G' = 7373 Pa before GCD and G' = 6276 Pa after GCD) are larger than the loss moduli (G'' = 587 Pa before GCD and G'' = 531 Pa after GCD) across the measured angular frequency range, indicating hydrogel-like characteristics before and after 100,000 cycles.[44] However, that a slight drop in G' occurs post GCD cycling may imply a slight decrease in average molecular weight.[29] It is worth emphasizing, however, that these changes are a result of GCD cycling, corresponding to the intrinsic instability of the hydrogel under charging and discharging conditions. With this set of data corresponding to cells prepared with Pris-CPE-K, we proceeded to evaluate the properties of the recycled samples, as described below.[45]

Comparative Evaluation of Re-CPE-Na Hydrogels. The CPE material was recycled by extraction from the electrode substrate with water, followed by purification via dialysis. As discussed in more detail below, based on the observation of Na 1s peaks in the wide sweep XPS spectrum of the recycled material (Figure 4a) one can determine that the compensating cations are Na^+ instead of K^+, most reasonably because of exchange with the NaCl electrolyte in the cell. We therefore refer to the recycled material as Re-CPE-Na. Indeed, we found that cation exchange occurs prior to GCD measurements by removing the CPE from the cell after equilibration with the electrolyte. This material will be termed Pris-CPE-Na to reflect that it does not undergo any possible degradation due to repeated charging/discharging cycles. It is also worth noting that the active materials in all the GCD experiments predominantly contain Na^+ counterions.

As shown in Figure 2a, the CV curves of Re-CPE-Na cells retain the quasirectangular shape characteristic of a pseudocapacitive material. These cells exhibit 83% of the average CV area observed for those prepared with Pris-CPE-K prior to GCD cycling and also similar electrochemical doping and dedoping efficiencies, (Figure 1a, Tables S2 and S3, Figures S14 and 15, and eq S3), albeit with a 24-mV shift of the oxidation onset potential toward more positive potentials. We further note that the current integrals of Re-CPE-Na cells before GCD are nearly identical with what is observed after the first 100,000 cycles GCD test with Pris-CPE-K cells, thus validating no impact by the recycling procedure. Moreover, we found that the b values calculated from Figure S8 are 0.98, an indication of a similar level of surface-controlled kinetics for cells fabricated with either Pris-CPE-K or Re-CPE-Na. Therefore, the recycling workup has no significant detrimental impact on the performance of the CPE.

EIS measurements were carried out to compare the internal resistances of Pris-CPE-K and Re-CPE-Na cells; see Figure 2c. These studies showed a statistically insignificant difference in R_{ct} values, 1.0 ± 0.6 Ω cm^{-2} (Pris-CPE-K) and 1.1 ± 0.8 Ω cm^{-2} (Re-CPE-Na). The FSW behavior of the electrodes is associated with a reflective boundary of blocking diffusion process as well as finite thickness of the gels network.[40,46] From the fitting model (Figure S9), the R_d value of Re-CPE-Na cells (15.2 ± 5.5 Ω cm^{-2}) is slightly larger than that of Pris-CPE-K cells (9.0 ± 1.9 Ω cm^{-2}) and the Warburg region, reflecting the ion diffusion length, becomes longer after recycling. In both cases, ionic diffusion is slightly different but is in accordance with the original capacitive behavior shown in the element FSW.

Figure 2d provides the logarithm of the module of impedance (Z) and phase change as a function of Log(frequency). The frequency of the Bode plot increases from left to right along the x-axis, which is opposite to the frequency migration in the Nyquist plot. In the range of the semicircle, Re-CPE-Na cells are characterized by a smaller phase angle, which is accompanied by a smaller α value, as shown in eq S2, thus suggesting that pseudocapacitance arises from combined diffusion and capacitive contributions.[47] Figure S16 demonstrates that the Z value of Re-CPE-Na cells is approximately 1.5 Ω larger than that of Pris-CPE-K cells, which is relatively insignificant compared to the difference in R_d. The R_d values of Re-CPE-Na (15.5 ± 5.5 Ω cm^{-2}) and Pris-CPE-K (9.0 ± 1.9 Ω cm^{-2}) cells are in line with the occurrence of ionic−electronic coupling and capacitive behaviors of both hydrogels.[48]

Figure 3a of cells prepared with Pris-CPE-K and Re-CPE-Na cells at current densities from 0.25 A g^{-1} to 20 A g^{-1}. We then selected 10 A g^{-1} for a subsequent round of 100,000 GCD cycles (Figure S10). In Figure 3b, the initial C_S = 26.3 ± 1.2 F g^{-1} for Re-CPE-Na cells reveals that the material retains the capacitance observed at the end of the first set of GCD measurements with cells prepared with CPE-K. We also note

https://doi.org/10.1021/acsami.3c13137
ACS Appl. Mater. Interfaces XXXX, XXX, XXX−XXX

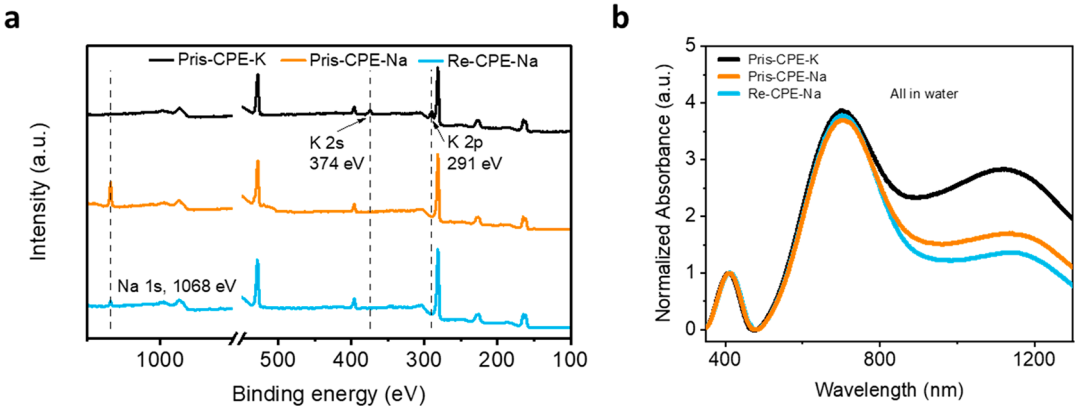

Figure 4. (a) Corresponding elemental wide sweep of XPS for Pris-CPE-K, Pris-CPE-Na and Re-CPE-Na. Note: Pris-CPE-Na in part a was obtained by immersing Pris-CPE-K at 2 M NaCl electrolyte in the electrochemical cell. (b) Optical absorption of Pris-CPE-K, Pris-CPE-Na, and Re-CPE-Na in water at 25 μg/mL.

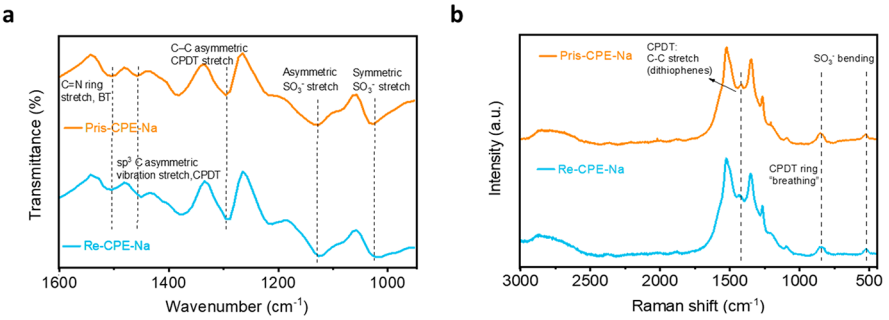

Figure 5. For Pris-CPE-Na and Re-CPE-Na, (a) ART-FTIR spectra and (b) Raman spectra, measured using an excitation laser of 532 nm.

that approximately 77% of the capacitance compared to the starting point of Re-CPE-Na was retained after a subsequent 100,000 GCD cycles. Furthermore, the Coulombic efficiency of Pris-CPE-K and Re-CPE-Na cells were both over 99% (Equation S4). In sum, the relative comparison demonstrates that the conjugated polyelectrolyte is recyclable as a pseudocapacitive material as determined by the negligible loss of performance as a result of the recycling procedure.[49]

Characterization of Pristine and Recycled CPEs. A series of experiments was designed to probe for possible changes in chemical structure post recycling. We first examined the optical absorption of Pris-CPE-K, Pris-CPE-Na, and Re-CPE-Na, see Figure 4b. Two absorption bands are observed below 800 nm, which correspond to the π to π^* (411 nm) and intramolecular charge transfer (ICT, 700 nm) transitions.[17] The broad absorption peak at 1100 nm is attributed to the presence of polaron species and is indicative of self-doping. One observes that the ratio of the polaron to ICT bands is higher for Pris-CPE-K relative to Re-CPE-Na; however, the spectral profiles of Pris-CPE-Na and Re-CPE-Na are similar to each other. Thus, the differences in doping level between Pris-CPE-K and Re-CPE-Na are reasonably attributed to the exchange of K^+ for Na^+, rather than changes in the backbone structure from GCD cycling experiments. Indeed, the optical absorption of Pris-CPE-K, Pris-CPE-Na and Re-CPE-Na in 0.1 M KOH (aq), conditions that dedope the backbone, are essentially indistinguishable (Figure S17 and Figure S18).

Wide sweep XPS was used to examine the elemental compositions. Figure 4a and Figure S19 show that the spectrum of Pris-CPE-K possesses a K 2p peak at 294.91 eV and a K 2s peak at 374.81 eV, whereas Pris-CPE-Na and Re-CPE-Na both exhibit a characteristic signature of Na 1s at 1068.02 eV. These changes are consistent with replacement of K^+ by Na^+ from the electrolyte. The carbon peaks in the energy range of 282 to 290 eV were fitted to C−C + C═C, C−S, and C═N contributions (Figure S20b). We determined percentage areas of 45 ± 2% and 43 ± 2% (C−C + C═C), 34 ± 2% and 36 ± 2% (C−S), and 20 ± 2% and 20 ± 2% (C═N), for Pris-CPE-Na and Re-CPE-Na, respectively. Similarly, we applied the fitting to sulfur, dividing it into S−O + S═O, S−N, and S−C regions, from which we obtained a ratio of 51:31:18 (RSD = 5) for Pris-CPE-Na and 50:32:18 (RSD = 5) for Re-CPE-Na, see Figure S20c. In short, XPS data show that the counterions of all the CPEs in GCD tests are Na^+ and the fittings of the carbon portion indicate that the backbone remains essentially unchanged.

The ATR-FTIR spectra of Pris-CPE-Na and Re-CPE-Na (Figure 5a) in the 1000−1600 cm^{-1} region show no discernible differences. The C−C asymmetric stretch appears within 1291−1296 cm^{-1} for all CPEs.[50] Additionally, the existence of the symmetric SO_3^- vibration and asymmetric SO_3^- stretch peaks indicates identical pendant groups. The Raman spectra of the samples (Figure 5b) feature a peak at 523 cm^{-1} that confirms similar sulfonate bending modes of Pris-CPE-Na as well as Re-CPE-Na, in line with the observations in ART-FTIR (Figure 5a). Overall, no differences can be observed in the ATR-FTIR and Raman spectra of Pris-CPE-Na and Re-CPE-Na, which gives us an indication that any changes in chemical structure are below the detection limits of these techniques after GCD cycling.

To improve the solubility and facilitate characterizations in solution, the counter cations of Pris-CPE-K and Re-CPE-Na

https://doi.org/10.1021/acsami.3c13137
ACS Appl. Mater. Interfaces XXXX, XXX, XXX−XXX

were exchanged for tetrabutylammonium (TBA) through ion exchange, as shown in Figure S3. We found nearly identical chemical shifts and integrals in the ^{1}H NMR spectra of both polymers (Figure S21), which also indicate negligible degradation of the backbone. No obvious differences could be detected in the SEM micrographs of Pris-CPE-Na and Re-CPE-Na that could report on morphological differences (Figure S22). The one difference noted comes from GPC analysis (Figure S23), where the number-average molecular weight of Re-CPE-TBA (100 kDa) is slightly lower than that of Pris-CPE-TBA (113 kDa). It is worth noting, however, that these differences may stem from the GCD cycling procedure, rather than the recycling process, and may be related to the slight decrease in G' and G'' observed in the rheological tests.

CONCLUSION

Herein, we demonstrate that CPE hydrogels used within the context of pseudocapacitive applications can be easily recycled by a simple procedure of extraction with water and purification via dialysis. Specifically, cells prepared with Pris-CPE-K in 2 M NaCl retained 80% of the original specific capacitance after 100,000 cycles of charging and discharging at a current density of 10 A g^{-1}. After recycling of the CPE, cells prepared with Re-CPE-Na display a specific capacitance similar to that observed at the final GCD cycle of the Pris-CPE-K cells. Moreover, Re-CPE-Na cells can retain 77% of their initial specific capacitance after 100,000 GCD cycles. In line with the retention of pseudocapacitive properties, we could not identify significant changes in the chemical structure of the backbone or the pendant sulfonate functional groups. To sum up, conjugated polyelectrolyte hydrogels provide innovative options for the design of energy storage materials in applications that take advantage of their unique properties, including self-healing capabilities, biocompatibility, and simple to apply processing and recycling options from aqueous media.

ASSOCIATED CONTENT

Supporting Information

The Supporting Information is available free of charge at https://pubs.acs.org/doi/10.1021/acsami.3c13137.

Detailed equations, cell assembly, recycling work up, and synthetic route; CV, EIS fittings and calculations of the model, GCD plots, and calculated doping and dedoping efficiency; and XPS peak fittings, UV−vis adsorption, NMR spectra, and GPC characterizations (PDF)

AUTHOR INFORMATION

Corresponding Author

Guillermo C. Bazan − *Departments of Chemistry and Chemical & Biomolecular Engineering, National University of Singapore, 119077, Singapore; Institute for Functional Intelligent Materials, National University of Singapore, 117544, Singapore; Singapore Centre for Environmental Life Sciences Engineering, Nanyang Technological University, 639798, Singapore; Department of Chemistry and Biochemistry, University of California, Santa Barbara, California 93106, United States;* orcid.org/0000-0002-2537-0310; Email: chmbgc@nus.edu.sg

Authors

Yan Jiang − *Departments of Chemistry and Chemical & Biomolecular Engineering, National University of Singapore, 119077, Singapore; Institute for Functional Intelligent Materials, National University of Singapore, 117544, Singapore;* orcid.org/0000-0002-0231-8552

Ricardo Javier Vázquez − *Departments of Chemistry and Chemical & Biomolecular Engineering, National University of Singapore, 119077, Singapore; Institute for Functional Intelligent Materials, National University of Singapore, 117544, Singapore; Singapore Centre for Environmental Life Sciences Engineering, Nanyang Technological University, 639798, Singapore; Department of Chemistry, Indiana University, Bloomington, Indiana 47405, United States;* orcid.org/0000-0003-3245-8123

Samantha R. McCuskey − *Departments of Chemistry and Chemical & Biomolecular Engineering, National University of Singapore, 119077, Singapore; Institute for Functional Intelligent Materials, National University of Singapore, 117544, Singapore; Singapore Centre for Environmental Life Sciences Engineering, Nanyang Technological University, 639798, Singapore*

Benjamin Rui Peng Yip − *Departments of Chemistry and Chemical & Biomolecular Engineering, National University of Singapore, 119077, Singapore; Institute for Functional Intelligent Materials, National University of Singapore, 117544, Singapore;* orcid.org/0009-0000-8379-5993

Glenn Quek − *Departments of Chemistry and Chemical & Biomolecular Engineering, National University of Singapore, 119077, Singapore; Institute for Functional Intelligent Materials, National University of Singapore, 117544, Singapore*

David Ohayon − *Departments of Chemistry and Chemical & Biomolecular Engineering, National University of Singapore, 119077, Singapore; Institute for Functional Intelligent Materials, National University of Singapore, 117544, Singapore*

Binu Kundukad − *Singapore Centre for Environmental Life Sciences Engineering, Nanyang Technological University, 639798, Singapore*

Xuehang Wang − *Department of Radiation Science and Technology, Delft University of Technology, Delft 2629 JB, Netherlands*

Complete contact information is available at: https://pubs.acs.org/10.1021/acsami.3c13137

Notes

The authors declare no competing financial interest.

ACKNOWLEDGMENTS

This work was supported by the Institute for Functional Intelligent Materials (I-FIM, Project No. EDUNC-33-18-279-V12) under the Ministry of Education, Singapore, by the National University of Singapore Start Up Grant R143-000-A97-133, and the Office of Naval Research (ONR-Global, N62909-22-1-2016).

REFERENCES

(1) Brousse, T.; Bélanger, D.; Long, J. W. To Be or Not To Be Pseudocapacitive? *J. Electrochem. Soc.* **2015**, *162* (5), A5185−A5189.

(2) Fleischmann, S.; Mitchell, J. B.; Wang, R.; Zhan, C.; Jiang, D. E.; Presser, V.; Augustyn, V. Pseudocapacitance: From Fundamental Understanding to High Power Energy Storage Materials. *Chem. Rev.* **2020**, *120* (14), 6738−6782.

(3) Choi, C.; Ashby, D. S.; Butts, D. M.; DeBlock, R. H.; Wei, Q.; Lau, J.; Dunn, B. Achieving High Energy Density and High Power

Density with Pseudocapacitive Materials. *Nat. Rev. Mater.* **2020**, *5* (1), 5−19.
(4) Jiang, Y.; Liu, J. Definitions of Pseudocapacitive Materials: A Brief Review. *Energy Environ. Mater.* **2019**, *2* (1), 30−37.
(5) Kim, J.; Kim, J. H.; Ariga, K. Redox-Active Polymers for Energy Storage Nanoarchitectonics. *Joule* **2017**, *1* (4), 739−768.
(6) Gogotsi, Y.; Penner, R. M. Energy Storage in Nanomaterials - Capacitive, Pseudocapacitive, or Battery-Like? *ACS Nano* **2018**, *12* (3), 2081−2083.
(7) Costentin, C.; Saveant, J. M. Energy Storage: Pseudocapacitance in Prospect. *Chem. Sci.* **2019**, *10* (22), 5656−5666.
(8) S. Mofarah, S.; Adabifiroozjaei, E.; Yao, Y.; Koshy, P.; Lim, S.; Webster, R.; Liu, X.; Khayyam Nekouei, R.; Cazorla, C.; Liu, Z.; Wang, Y.; Lambropoulos, N.; Sorrell, C. C. Proton-Assisted Creation of Controllable Volumetric Oxygen Vacancies in Ultrathin $CeO_{(2-X)}$ for Pseudocapacitive Energy Storage Applications. *Nat. Commun.* **2019**, *10* (1), 2594.
(9) Bryan, A. M.; Santino, L. M.; Lu, Y.; Acharya, S.; D'Arcy, J. M. Conducting Polymers for Pseudocapacitive Energy Storage. *Chem. Mater.* **2016**, *28* (17), 5989−5998.
(10) Amin, K.; Ashraf, N.; Mao, L.; Faul, C. F. J.; Wei, Z. Conjugated Microporous Polymers for Energy Storage: Recent Progress and Challenges. *Nano Energy* **2021**, *85*, 105958.
(11) Sun, H.; Guo, X.; Facchetti, A. High-Performance n-Type Polymer Semiconductors: Applications, Recent Development, and Challenges. *Chem.* **2020**, *6* (6), 1310−1326.
(12) Quek, G.; Roehrich, B.; Su, Y.; Sepunaru, L.; Bazan, G. C. Conjugated Polyelectrolytes: Underexplored Materials for Pseudocapacitive Energy Storage. *Adv. Mater.* **2022**, *34* (22), No. e2104206.
(13) Mai, C.-K.; Russ, B.; Fronk, S. L.; Hu, N.; Chan-Park, M. B.; Urban, J. J.; Segalman, R. A.; Chabinyc, M. L.; Bazan, G. C. Varying the Ionic Functionalities of Conjugated Polyelectrolytes Leads to Both p- and n-Type Carbon Nanotube Composites for Flexible Thermoelectrics. *Energy Environ. Sci.* **2015**, *8* (8), 2341−2346.
(14) Cui, Q.; Bazan, G. C. Narrow Band Gap Conjugated Polyelectrolytes. *Acc. Chem. Res.* **2018**, *51* (1), 202−211.
(15) Wu, Q.; He, T.; Zhang, Y.; Zhang, J.; Wang, Z.; Liu, Y.; Zhao, L.; Wu, Y.; Ran, F. Cyclic Stability of Supercapacitors: Materials, Energy Storage Mechanism, Test Methods, and Device. *J. Mater. Chem. A* **2021**, *9* (43), 24094−24147.
(16) Scaccabarozzi, A. D.; Basu, A.; Anies, F.; Liu, J.; Zapata-Arteaga, O.; Warren, R.; Firdaus, Y.; Nugraha, M. I.; Lin, Y.; Campoy-Quiles, M.; Koch, N.; Muller, C.; Tsetseris, L.; Heeney, M.; Anthopoulos, T. D. Doping Approaches for Organic Semiconductors. *Chem. Rev.* **2022**, *122* (4), 4420−4492.
(17) Giovannitti, A.; Maria, I. P.; Hanifi, D.; Donahue, M. J.; Bryant, D.; Barth, K. J.; Makdah, B. E.; Savva, A.; Moia, D.; Zetek, M.; Barnes, P. R. F.; Reid, O. G.; Inal, S.; Rumbles, G.; Malliaras, G. G.; Nelson, J.; Rivnay, J.; McCulloch, I. The Role of the Side Chain on the Performance of n-Type Conjugated Polymers in Aqueous Electrolytes. *Chem. Mater.* **2018**, *30* (9), 2945−2953.
(18) Tang, H.; Liang, Y.; Liu, C.; Hu, Z.; Deng, Y.; Guo, H.; Yu, Z.; Song, A.; Zhao, H.; Zhao, D.; Zhang, Y.; Guo, X.; Pei, J.; Ma, Y.; Cao, Y.; Huang, F. A Solution-Processed n-Type Conducting Polymer with Ultrahigh Conductivity. *Nature* **2022**, *611* (7935), 271−277.
(19) Wang, A.; Tan, R.; Breakwell, C.; Wei, X.; Fan, Z.; Ye, C.; Malpass-Evans, R.; Liu, T.; Zwijnenburg, M. A.; Jelfs, K. E.; McKeown, N. B.; Chen, J.; Song, Q. Solution-Processable Redox-Active Polymers of Intrinsic Microporosity for Electrochemical Energy Storage. *J. Am. Chem. Soc.* **2022**, *144* (37), 17198−17208.
(20) Tan, P.; Wang, H.; Xiao, F.; Lu, X.; Shang, W.; Deng, X.; Song, H.; Xu, Z.; Cao, J.; Gan, T.; Wang, B.; Zhou, X. Solution-Processable, Soft, Self-Adhesive, and Conductive Polymer Composites for Soft Electronics. *Nat. Commun.* **2022**, *13* (1), 358.
(21) Kumar, N.; Gajraj, V.; Rameshbabu, R.; Mangalaraja, R. V.; Joshi, N. C.; Priyadarshi, N. Redox Additive Electrolyte Assisted Promising Pseudocapacitance from Strictly 1D and 2D Blended Structures of MnO_2/rGO. *Mater. Charact.* **2022**, *189*, 111991.
(22) Neekzad, N.; Kowsari, E.; Najafi, M. D.; Reza Naderi, H.; Chinnappan, A.; Ramakrishna, S.; Haddadi-Asl, V. Pseudocapacitive Performance of Surface Functionalized Halloysite Nanotubes Decorated Green Additive Ionic Liquid Modified with ATP and POAP for Efficient Symmetric Supercapacitors. *J. Mol. Liq.* **2021**, *342*, 116962.
(23) McCulloch, I.; Chabinyc, M.; Brabec, C.; Nielsen, C. B.; Watkins, S. E. Sustainability Considerations for Organic Electronic Products. *Nat. Mater.* **2023**, *22*, 1304.
(24) Kirchhofer, N. D.; McCuskey, S. R.; Mai, C. K.; Bazan, G. C. Anaerobic Respiration on Self-Doped Conjugated Polyelectrolytes: Impact of Chemical Structure. *Angew. Chem., Int. Ed.* **2017**, *56* (23), 6519−6522.
(25) Quek, G.; Su, Y.; Donato, R. K.; Vázquez, R. J.; Marangoni, V. S.; Ng, P. R.; Costa, M. C. F.; Kundukad, B.; Novoselov, K. S.; Neto, A. H. C.; Bazan, G. C. Pseudocapacitive Conjugated Polyelectrolyte/2D Electrolyte Hydrogels with Enhanced Physico-Electrochemical Properties. *Adv. Electron. Mater.* **2022**, *8* (5), 2100942.
(26) McCuskey, S. R.; Chatsirisupachai, J.; Zeglio, E.; Parlak, O.; Panoy, P.; Herland, A.; Bazan, G. C.; Nguyen, T. Q. Current Progress of Interfacing Organic Semiconducting Materials with Bacteria. *Chem. Rev.* **2022**, *122* (4), 4791−4825.
(27) McCuskey, S. R.; Su, Y.; Leifert, D.; Moreland, A. S.; Bazan, G. C. Living Bioelectrochemical Composites. *Adv. Mater.* **2020**, *32* (24), No. e1908178.
(28) Su, Y.; McCuskey, S. R.; Leifert, D.; Moreland, A. S.; Zhou, L.; Llanes, L. C.; Vazquez, R. J.; Sepunaru, L.; Bazan, G. C. A Living Biotic−Abiotic Composite that can Switch Function Between Current Generation and Electrochemical Energy Storage. *Adv. Funct. Mater.* **2021**, *31* (6), 2007351.
(29) Vázquez, R. J.; Quek, G.; McCuskey, S. R.; Llanes, L.; Kundukad, B.; Wang, X.; Bazan, G. C. Increasing the Molecular Weight of Conjugated Polyelectrolytes Improves the Electrochemical Stability of Their Pseudocapacitor Gels. *J. Mater. Chem. A* **2022**, *10* (40), 21642−21649.
(30) Bhar, M.; Bhattacharjee, U.; Sarma, D.; Krishnamurthy, S.; Yalamanchili, K.; Mahata, A.; Martha, S. K. A Novel and Sustainable Approach to Enhance the Li-Ion Storage Capability of Recycled Graphite Anode from Spent Lithium-Ion Batteries. *ACS Appl. Mater. Interfaces* **2023**, *15*, 26606.
(31) Jehanno, C.; Alty, J. W.; Roosen, M.; De Meester, S.; Dove, A. P.; Chen, E. Y.; Leibfarth, F. A.; Sardon, H. Critical Advances and Future Opportunities in Upcycling Commodity Polymers. *Nature* **2022**, *603* (7903), 803−814.
(32) Ciez, R. E.; Whitacre, J. F. Examining Different Recycling Processes for Lithium-Ion Batteries. *Nat. Sustain* **2019**, *2* (2), 148−156.
(33) Tan, S. T. M.; Quill, T. J.; Moser, M.; LeCroy, G.; Chen, X.; Wu, Y.; Takacs, C. J.; Salleo, A.; Giovannitti, A. Redox-Active Polymers Designed for the Circular Economy of Energy Storage Devices. *ACS Energy Lett.* **2021**, *6* (10), 3450−3457.
(34) Mai, C. K.; Zhou, H.; Zhang, Y.; Henson, Z. B.; Nguyen, T. Q.; Heeger, A. J.; Bazan, G. C. Facile Doping of Anionic Narrow-Band-Gap Conjugated Polyelectrolytes During Dialysis. *Angew. Chem., Int. Ed.* **2013**, *52* (49), 12874−12878.
(35) Ohayon, D.; Renn, D.; Wustoni, S.; Guo, K.; Druet, V.; Hama, A.; Chen, X.; Maria, I. P.; Singh, S.; Griggs, S.; Schroeder, B. C.; Rueping, M.; McCulloch, I.; Inal, S. Interactions of Catalytic Enzymes with n-Type Polymers for High-Performance Metabolite Sensors. *ACS Appl. Mater. Interfaces* **2023**, *15* (7), 9726−9739.
(36) Mathis, T. S.; Kurra, N.; Wang, X.; Pinto, D.; Simon, P.; Gogotsi, Y. Energy Storage Data Reporting in Perspective—Guidelines for Interpreting the Performance of Electrochemical Energy Storage Systems. *Adv. Energy Mater.* **2019**, *9* (39), 1902007.
(37) Pu, X.; Zhao, D.; Fu, C.; Chen, Z.; Cao, S.; Wang, C.; Cao, Y. Understanding and Calibration of Charge Storage Mechanism in Cyclic Voltammetry Curves. *Angew. Chem., Int. Ed.* **2021**, *60* (39), 21310−21318.

https://doi.org/10.1021/acsami.3c13137
ACS Appl. Mater. Interfaces XXXX, XXX, XXX−XXX

(38) Laschuk, N. O.; Easton, E. B.; Zenkina, O. V. Reducing the Resistance for the Use of Electrochemical Impedance Spectroscopy Analysis in Materials Chemistry. *RSC Adv.* **2021**, *11* (45), 27925−27936.
(39) de Pauli, M.; Gomes, A. M. C.; Cavalcante, R. L.; Serpa, R. B.; Reis, C. P. S.; Reis, F. T.; Sartorelli, M. L. Capacitance Spectra Extracted from EIS by a Model-Free Generalized Phase Element Analysis. *Electrochim. Acta* **2019**, *320*, 134366.
(40) Lazanas, A. C.; Prodromidis, M. I. Electrochemical Impedance Spectroscopy—A Tutorial. *ACS meas. sci. au* **2023**, *3*, 162.
(41) Song, J.; Bazant, M. Z. Effects of Nanoparticle Geometry and Size Distribution on Diffusion Impedance of Battery Electrodes. *J. Electrochem. Soc.* **2013**, *160* (1), A15−A24.
(42) Boukamp, B. Electrochemical Impedance Spectroscopy in Solid State Ionics: Recent Advances. *Solid State Ion.* **2004**, *169* (1−4), 65−73.
(43) Wu, R.; Paulsen, B. D.; Ma, Q.; McCulloch, I.; Rivnay, J. Quantitative Composition and Mesoscale Ion Distribution in p-Type Organic Mixed Ionic-Electronic Conductors. *ACS Appl. Mater. Interfaces* **2023**, *15*, 30553.
(44) Fong, K. D.; Wang, T.; Smoukov, S. K. Multidimensional Performance Optimization of Conducting Polymer-based Supercapacitor Electrodes. *Sustain. Energy Fuels* **2017**, *1* (9), 1857−1874.
(45) Harper, G.; Sommerville, R.; Kendrick, E.; Driscoll, L.; Slater, P.; Stolkin, R.; Walton, A.; Christensen, P.; Heidrich, O.; Lambert, S.; Abbott, A.; Ryder, K.; Gaines, L.; Anderson, P. Recycling Lithium-Ion Batteries from Electric Vehicles. *Nature* **2019**, *575* (7781), 75−86.
(46) Oldenburger, M.; Bedürftig, B.; Gruhle, A.; Grimsmann, F.; Richter, E.; Findeisen, R.; Hintennach, A. Investigation of the Low Frequency Warburg Impedance of Li-Ion Cells by Frequency Domain Measurements. *J. Energy Storage* **2019**, *21*, 272−280.
(47) Wang, S.; Zhang, J.; Gharbi, O.; Vivier, V.; Gao, M.; Orazem, M. E. Electrochemical Impedance Spectroscopy. *Nat. Rev. Methods Primers* **2021**, *1* (1), 41.
(48) Wu, R.; Matta, M.; Paulsen, B. D.; Rivnay, J. Operando Characterization of Organic Mixed Ionic/Electronic Conducting Materials. *Chem. Rev.* **2022**, *122* (4), 4493−4551.
(49) Liu, T.; Finn, L.; Yu, M.; Wang, H.; Zhai, T.; Lu, X.; Tong, Y.; Li, Y. Polyaniline and Polypyrrole Pseudocapacitor Electrodes with Excellent Cycling Stability. *Nano Lett.* **2014**, *14* (5), 2522−2527.
(50) Cao, D. X.; Leifert, D.; Brus, V. V.; Wong, M. S.; Phan, H.; Yurash, B.; Koch, N.; Bazan, G. C.; Nguyen, T.-Q. The Importance of Sulfonate to the Self-Doping Mechanism of the Water-Soluble Conjugated Polyelectrolyte PCPDTBT-SO_3K. *Mater. Chem. Front.* **2020**, *4* (12), 3556−3566.

https://doi.org/10.1021/acsami.3c13137
ACS Appl. Mater. Interfaces XXXX, XXX, XXX−XXX